IJDAR (2003) 6: 115–125
Digital Object Identifier (DOI) 10.1007/s10032-003-0105-0

International Journal on IJDAR Document Analysis and Recognition

Matching of graphical symbols in line-drawing images using angular signature information

S. Tabbone, L. Wendling, K. Tombre

LORIA, B.P. 239, 54506 Vandœuvre-lès-Nancy Cedex, France

Received: 7 October 2002 / Accepted: 1 December 2002
Published online: 4 July 2003 –

Abstract. In this paper, a method for matching complex objects in line-drawings is presented. Our approach is based on the notion of $\mathcal{F}$-signatures, which are a special kind of histogram of forces [17,19,28]. Such histograms have low time complexity and describe signatures that are invariant to fundamental geometrical transformations such as scaling, translation, symmetry, and rotation. This article presents a new application of this notion in the field of symbol identification and recognition. To improve the efficiency of matching, we propose using an approximation of the $\mathcal{F}$-signature from Fourier series and the associated matching.

Key words: $\mathcal{F}$-signatures – Fourier series – Symbol recognition – Graphics recognition

1 Introduction

In this paper, which is a thorough extension of work presented in [25], we propose a method for the recognition of complex symbols in technical drawings based on the notion of $\mathcal{F}$-signatures, which is a particular histogram of forces [17,19,28]. The aim is to define a signature for each object found in a line-drawing.

A preliminary step consists in defining a set of samples that will be used as models for the symbols to be found. The signatures used allow us to represent the attraction forces that are exerted between the parts of an object following a set of directions and are discriminant features for achieving an accurate classification. Furthermore, such a signature has low time complexity and allows us to recover fundamental geometric tranformations like rotation, translation, scale factor (considering only the shape of the $\mathcal{F}$-signature), and symmetry.

A brief overview of pattern recognition approaches in the field of symbol recognition is given in Sect. 2. Then the notion of histogram of forces and its properties are recalled in Sect. 3. An approximation of such signatures is performed to achieve efficient matching by taking directly into account the rotation factor (Sect. 4). Experimental studies and a discussion about the advantages and limitations of our approach are given in Sect. 5.

Correspondence to: S. Tabbone (e-mail: tabbone@loria.fr)

2 Related work

Despite the large quantity of technical documentation floating around, there have been relatively few studies on how to integrate graphics-rich information into an indexing process. For instance, in this case, it is crucial to be able to index not only on textual labels but also on symbols or even larger graphical components. This in turn requires efficient ways of recognizing symbols [5] or at least identifying symbol signatures. The relatively low volume of work in this area is probably due to the huge variety of symbols encountered, depending on the type of documentation to be processed. Also, the large variability of the symbols encountered in technical drawings requires the use of invariant descriptors for identification and recognition and hence the development of efficient and useful invariants [29].

Simple geometrical characteristics have been used to classify the shape of objects: the degree of compactness and the degree of ellipticity (the axes being given by the moments of order 0 to 2 [26]). Nevertheless, these features and their combination often yield inconsistent results. The perimeter has a strong effect on the computation of compactness, and when the drawing is not sharp, the use of such a feature may yield a bad classification. Furthermore, approaches based on feature descriptors [3, 10,14] are sensitive to noise and are not robust to occlusion.

A polygonal approximation of the objects could be a solution to this problem. However, it induces loss of information, which may result in lower recognition rates. The degree of ellipticity is also not suited to the classification of this type of object. Maes [16], for example, has presented a string-matching technique to the problem of recognizing and classifying polygons; but the strengh of this

method is limited when the polygonal approximation of the object is inconsistent. Gerdes et al. [9] have proposed another approach based on contour-oriented 2D object recognition that is more robust to the polygonal approximation inconsistency. Its main drawback is its time complexity, especially when many models must be identified. The generalized Hough transform [1] is also a useful technique for shape recognition, but its drawbacks — computation time and storage requirements — are substantial. Even though improvements have been proposed [11], the approach remains complex when many models must be characterized. For a thorough survey of the various techniques and descriptors that may be used, the reader may refer to [15].

From a more practical point of view, when addressing specific applications, some ad hoc systems have been designed. Syeda-Mahmood uses an adaptation of the topological rules for representing the world of blocks to successfully index a database of technical maintenance drawings [23]. Her approach is based on a structural representation, a labeling step to give all the hypotheses, and a discrete relaxation step. The symbols are not actually recognized, but sufficient structural information is identified for the problem addressed. In another system, designed at the Boeing company, low-level text and graphics recognition tools have been successfully used in a customized interactive environment to provide a visual information retrieval system [2]. Once again, although very interesting for the practical problem addressed, the approach remains ad hoc and does not pretend to offer a generic solution to the problem of shape recognition.

In the specific area of technical drawings, Fränti et al. [8] have proposed using the Hough transform for content-based matching in line-drawing images. The method presented in this paper is another approach to solving this generic problem. We take into account complex shapes without setting any constraints on the contours, which can be closed or not. Whereas Fourier descriptors [12, 21, 22] require computing the centroid of the shapes under consideration, in order to optimize the results of the transformation, we do not set any such constraint either.

3 Signature of a complex object

3.1 $\mathcal{F}$-signature computation

In this section, we recall the scheme for computing the $\mathcal{F}$-signature of a binary graphical object, which is a particular histogram of forces [17, 19, 28]. A histogram of forces can be assumed to be the calculation of all the forces exerted among the pixels of the same object. Let φ_r be the map from $\mathbb{R}$ into $\mathbb{R}_+$, null on $\mathbb{R}_-$ and continuous on $\mathbb{R}_+^*$, such that:

$$\forall d \in \mathbb{R}_+^*,\ \varphi_r(d) = 1/d^r \tag{1}$$

Let a_1 and a_2 be two points of $\mathbb{R}^2$ and d the distance between a_1 and a_2. The attraction force is given by $\varphi(d)$. The value of r defines the type of force to be used. For example, $r = 0$ corresponds to constant forces, and $r = 2$ refers to the gravitational attraction. The generalization to the entire object can be done by using all pairs of pixels. However, the histogram obtained in this way can be noisy and strongly dependent on the angle threshold of the histogram – as is the case in [13, 20] – for the histogram of angles, with a complexity of $\mathcal{O}\left(n^2\right)$ arctan, with n being the number of points of the considered object. To overcome this problem, the use of straight lines following a set of directions θ is considered, and the method handles segments (see Fig. 1) in order to decrease the processing time. The extracted forces are calculated between segments, i.e., the attraction force of one segment with respect to another segment is computed. Let I_1 and I_2 be two segments carried by the same straight line, $|I_1|$ and $|I_2|$ their respective lengths, and $D^\theta_{I_1 I_2}$ the distance between I_1 and I_2. The attraction force from I_1 to I_2 is given by

$$f_r(|I_1|, D^\theta_{I_1 I_2}, |I_2|) = \int_0^{|I_2|} \int_{D^\theta_{I_1 I_2}+|I_2|}^{|I_1|+D^\theta_{I_1 I_2}+|I_2|} \varphi_r(u-v)dvdu \tag{2}$$

For example, the calculation of f_0 corresponds to $|I_1| \times |I_2|$ when I precedes J and to $|I_1|^2/2$, assuming that I_1 and I_2 are superimposed; using f_2, if I_1 precedes I_2, the force is given by $\ln \frac{(D^\theta_{I_1 I_2}+|I_1|)(D^\theta_{I_1 I_2}+|I_2|)}{D^\theta_{I_1 I_2}(D^\theta_{I_1 I_2}+|I_1|+(D^\theta_{I_1 I_2}+|I_2|))}$.

Let A be an object of the plane; a pencil of parallel straight lines of angle θ from the orthogonal frame of the image, which entirely describes A, can be defined. Let $\mathcal{D}^\theta_\eta$ be one line; the set of segments of A carried by this straight line corresponds to $A_\theta(\eta) = \cup\{I_i\}_{i=1,n}$. The mutually attractive force between these segments is given by:

$$F(\theta, A_\theta(\eta), A_\theta(\eta)) = \sum_{i\in 1..n} \sum_{j\in 1..n} f_r(|I_i|, D^\theta_{I_i I_j}, |I_j|) \tag{3}$$

All the pencils of lines $\mathcal{D}^\eta_\theta$ of the plane that entirely describe A are then considered.

$$F^{AA}| \quad \begin{array}{l} \mathbb{R} \to \mathbb{R}_+, \\ \theta \longmapsto \int_{-\infty}^{+\infty} F(\theta, A_\theta(v), A_\theta(v))dv \end{array} \tag{4}$$

In the discrete case, the calculation of $F^{AA}(\theta)$ provides an evaluation of the forces exerted by the object on itself in the direction θ. The calculation of F^{AA} following the set of angles θ_i ($\theta_i \in [-\pi, +\pi[$) defines the $\mathcal{F}^A$ signature of the object A.

3.2 Properties of $\mathcal{F}$-signatures

3.2.1 Shape discrimination. The $\mathcal{F}$-signature gives more substantial information about the shape of the object than a simple criterion of compactness degree defined by the classical formula $C = \frac{4*\pi S}{P^2}$, with P the perimeter and S the surface. For example, Table 1 shows the behavior of both the $\mathcal{F}$-signature and the compactness of

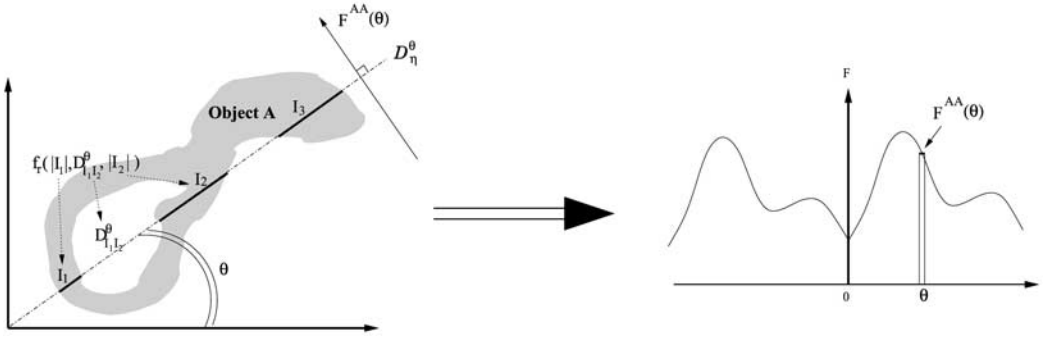

Fig. 1. Definition of an $\mathcal{F}$-signature

Table 1. Comparison between $\mathcal{F}$-signature and compactness degree of elliptical shapes. The equation of the ellipse is defined by $\frac{x^2}{a^2} + \frac{x^2}{b^2} = 1$. The compactness is defined by $C \approx \frac{2ab}{a^2+b^2}$

	$(a = b = 1)$	$(a = 2b)$	$(a = 4b)$	$(a = 8b)$
	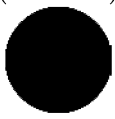			
C	1	$\frac{4}{5}$	$\frac{8}{17}$	$\frac{16}{65}$
$\mathcal{F}$-S	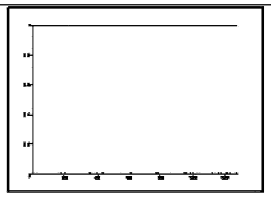	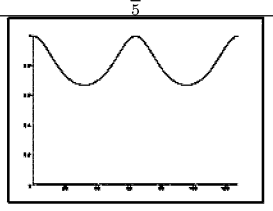	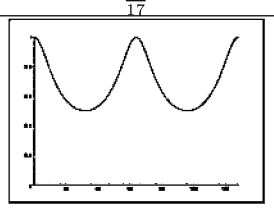	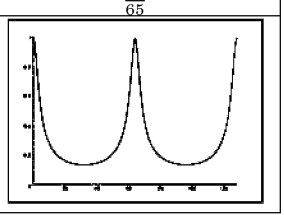

a circle degraded into an ellipse (the x-axis corresponds to the angle $\theta \in [-\pi, \pi[$ and the y-axis to $F^{AA}(\theta)$). In this case, both measures are discriminant. The objects are represented in black and the background in white.

However, the compactness degree does not give any information about the spatial representation of the object. Indeed, we can easily assume that the compactness degrees of the two images in Fig. 2 are very similar, but the objects have a very different spatial representation. This is shown by their $\mathcal{F}$-signature, which is in fact very discriminant.

3.2.2 Geometric properties. The aim of our approach is to classify similar objects independently of their location, orientation, and size in a document. Thus it is important to have a feature able to take into account fundamental geometric properties like translation, rotation, and scale factor. By definition, in the continuous case, the properties of F allow us to easily find such geometric transformations [17,19]:

– **Translation:** only the information of the object is processed independently of its location in the frame of the image. Let $T_{\boldsymbol{u}}$ be a translation of vector $\boldsymbol{u}$:

$$F^{AA}(\theta) = F^{T_{\boldsymbol{u}}(A)T_{\boldsymbol{u}}(A)}(\theta) \tag{5}$$

– **Symmetry:** the forces exerted on an object are the same following two opposite directions:

$$F^{AA}(\theta) = F^{AA}(\pi - \theta) \tag{6}$$

– **Scale factor:** only the shape of the $\mathcal{F}$-signatures is considered. If a scale factor is applied to an object, its histogram will be stretched. In such a case, the forces are multiplied by a value that depends on r and on the scale factor:

$$f_r(k|I|, kD^{\theta}_{IJ}, k|J|) = k^{2-r} f_r(|I|, D^{\theta}_{IJ}, |J|) \tag{7}$$

– **Rotation:** when a rotation is applied to an object, the histogram is shifted, as our approach is isotropic. Let θ be a direction and r be a rotation of angle θ' applied to an object A; this gives us:

$$F^{AA}(\theta) = F^{r(A,\theta')r(A,\theta')}(\theta + \theta') \tag{8}$$

These properties are also valid in the discrete case, with weak error variations, due to both the histogram and the sampling step. Figure 3 presents an object rotated by steps of $\pi/8$ and the associated signatures.

We will see in Sect. 4 how to find the angle of rotation and the scale factor from the $\mathcal{F}$-signature of a binary object.

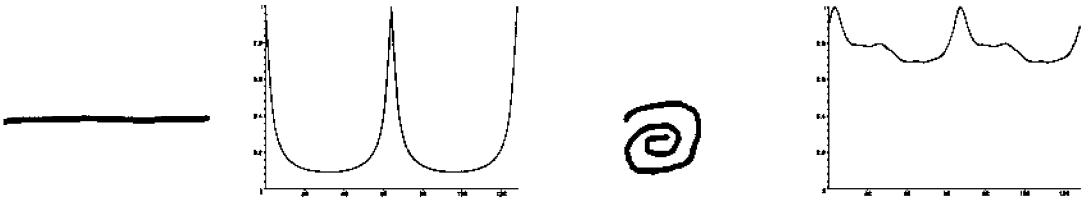

Fig. 2. $\mathcal{F}$-signature (θ between $[0, 2\pi[$) and spatial representation

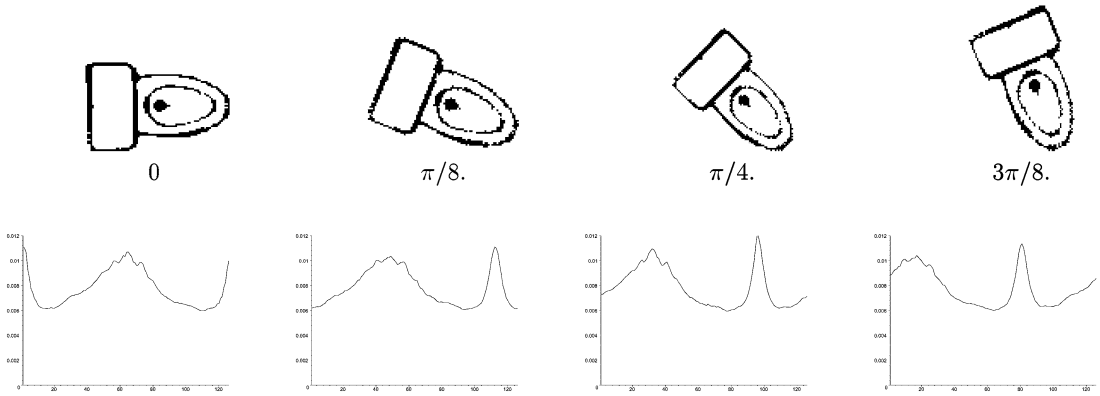

Fig. 3. Effect of object rotation on the signatures

Table 2. Distances between $\mathcal{F}$-signatures of original and degraded images with increasing noise

I	I_{5s}	I_{10s}	I_{15s}	I_{30s}
max	0.069	0.237	0.659	2.383
$\bar{\mu}$	0.043	0.13	0.315	1.185
RMS	$1.8 \cdot 6^{-5}$	$6 \cdot 10^{-5}$	$2 \cdot 10^{-4}$	$7.6 \cdot 10^{-4}$

3.3 Robustness to deformation

Various kinds of noise have been applied to a synthetic disk to test the robustness of our approach. Table 2 presents the variations between the original signature and the degraded signatures in terms of percentage (maximal difference, mean difference, and root mean square error). The small differences obtained show the robustness of our approach.

The robustness to noise stems from function f, which is continuous even if the segments are split into several parts, and to the summing effect of F^{AA}. Thus, weak disparities with respect to the global structure of the object have only a limited influence on the shape of the global $\mathcal{F}$-signature of the object.

3.4 Complexity

The time complexity for computing a histogram of forces is in $\mathcal{O}(p \cdot n\sqrt{(n)})$, where n is the number of pixels of the image and p the number of digitalization steps of the histogram [19]. This boundary is reached for very highly textured images. In our approach, the complexity is in $\mathcal{O}(p \cdot n)$ when using constant-force histograms and also in most cases when using other force histograms. Experimental results have shown that a good threshold is to set p at 128 (see Sect. 4.2).

For efficiency reasons, Bresenham's algorithm [4] is used in our implementation as it is a fast method that minimizes error in drawing lines on integer grid points. It approximates line segments defined by rational coefficients using only integral points. Bresenham's algorithm is applied only to one line to store the horizontal and vertical shifts representing a line scanning the image following the direction θ. These shifts are used to define the pencil of lines allowing one to scan the whole image (with this approach and for a given orientation θ, any given pixel is processed by only one line). The p directions are then processed to define the $\mathcal{F}$-signature.

4 Matching process

4.1 Context of our study

The histogram of forces gives a powerful, albeit discrete, representation of the object. In a large database, storing the signatures of each sample would require a considerable amount of memory. Moreover, matching the signature of a new sample with all those containted in the database (with no optimization) might need a high processing time.

Our aim is therefore to approximate the $\mathcal{F}$-signatures with a mathematical formula and to classify them in order to decrease memory requirements and to have an accurate indexing process.

Table 3. Distance variations following increasing values of p

I	I_{5s}	I_{10s}	I_{15s}	I_{30s}
				
$p = 16$	$4 \cdot 10^{-4}$	$12 \cdot 10^{-4}$	$27 \cdot 10^{-4}$	$127 \cdot 10^{-4}$
$p = 32$	$4 \cdot 10^{-4}$	$13 \cdot 10^{-4}$	$29 \cdot 10^{-4}$	$127 \cdot 10^{-4}$
$p = 64$	$4 \cdot 10^{-4}$	$13 \cdot 10^{-4}$	$30 \cdot 10^{-4}$	$128 \cdot 10^{-4}$
$p = 128$	$4 \cdot 10^{-4}$	$13 \cdot 10^{-4}$	$31 \cdot 10^{-4}$	$129 \cdot 10^{-4}$
$p = 256$	$4 \cdot 10^{-4}$	$13 \cdot 10^{-4}$	$31 \cdot 10^{-4}$	$129 \cdot 10^{-4}$
$p = 512$	$4 \cdot 10^{-4}$	$13 \cdot 10^{-4}$	$31 \cdot 10^{-4}$	$129 \cdot 10^{-4}$

4.2 Matching discrete signatures

We have matched the discrete signature of a particular object with the signatures of the images belonging to the database. The signatures are normalized by the area to take into account only the shape of the signature and to be able to match similar objects at different scales. The distance between two signatures is computed using a simple similarity ratio. Let $\bar{\mathcal{F}}^A$, $\bar{\mathcal{F}}^B$ be the normalized signatures of objects A and B, respectively; we compute the similarity ratio SR (by definition, if an object exists, its signature is never empty). This ratio depends on the scale factor and on the angle of rotation between the two signatures. The number of circular shifts CR applied to one signature to reach the better match is used to compute an approximation of the angle of rotation of the object. Let p be the number of direction. The final expression of SR is given by

$$SR(\bar{\mathcal{F}}^A, \bar{\mathcal{F}}^B) = 1. - \max_{CR \in [0,\pi[} \frac{\sum_{\theta=0,p} \min\left(\bar{\mathcal{F}}^A_\theta, \bar{\mathcal{F}}^B_{(\theta+CR)\%p}\right)}{\sum_{\theta=0,p} \max\left(\bar{\mathcal{F}}^A_\theta, \bar{\mathcal{F}}^B_{(\theta+CR)\%p}\right)} \quad (9)$$

SR is reached following the arg max, which maximizes CR by maximizing the classical Tanimoto index (min over max).

Table 3 gives the influence of the discretization factor p on SR. The first image is compared to the others. The value of SR is given for several values of p. Results show that a value of p set at 128 is a good threshold (greater values gave only a difference of about 10^{-5}).

An experimental study has shown that such a criterion yields good results in most cases for our study [25]. Nevertheless, to have a better robust distance measure and to overcome the computing of similarity ratios following circular shifts, we have studied the properties of Fourier series of $\mathcal{F}$-signatures. Furthermore, an approximation of the signature using Fourier series decreases the required storage space and improves the matching process.

4.3 Fourier series of $\mathcal{F}$-signatures

As the signature is periodic, with a period π (see Sect. 3.2), the Fourier series are well suited as descriptors and provide good noise reduction in the matching process. Let T be the number of points of the $\mathcal{F}$-signature.

$$\begin{aligned} x_k(t) &= a_0 + \sum_{k=1}^{K} \left(a_k \cos k\tfrac{2\pi}{T}t + b_k \sin k\tfrac{2\pi}{T}t\right) \\ &= a_0 + \sum_{k=1}^{K} c_k \cos\left(k\omega_0 t + \varphi_k\right) \end{aligned} \quad (10)$$

with

$$\begin{aligned} c_k &= \sqrt{a_k^2 + b_k^2} \\ \varphi_k &= -\tan^{-1}\left(\tfrac{b_k}{c_k}\right) \end{aligned} \quad (11)$$

That is, in the continuous case

$$\begin{aligned} a_k &= \tfrac{2}{T}\int_0^T x(t)\cos(k\omega_0 t)dt \\ b_k &= \tfrac{2}{T}\int_0^T x(t)\sin(k\omega_0 t)dt \\ a_0 &= \tfrac{1}{T}\int_0^T x(t)dt \end{aligned} \quad (12)$$

with $\omega_0 = \frac{2\pi}{T}$ being the frequency.

As the c_k factors are invariant to rotation of the signature modulo π, we use a simple metric to match two signals $x_k(t)$ and $x_k^{'}(t)$:

$$M(x_k(t), x_k^{'}(t)) = \sum_{k=1,K} |c_k - c_k^{'}| \quad (13)$$

By definition, K corresponds to the fitting degree of the Fourier series with respect to the discrete signature. For every new harmonic, we estimate the global fitting error (quadratic error between the discrete signature and the continuous signal). The value of K therefore depends on the discrete signature and on an accuracy threshold that is predefined for the whole reference set.

4.4 Improving classification using sets of samples for each cluster

To improve our approach and to have a more robust recognition process, we used a set of more or less degraded samples (around ten per cluster) for each cluster. For example, the sets of $\mathcal{F}$-signatures for the clusters "WC" and "Washbasin" are presented in Fig. 4. The shapes of the signatures are close to each other. For the sake of presentation, the signatures are centered following scale factor and rotations.

For each cluster we have defined a minimal, a maximal, and a median $\mathcal{F}$-signature. Let $C_i = \{A_1^i, A_2^i, \ldots, A_i^n\}$ be a cluster composed of n samples A_j^i; this gives us

$$\mathcal{F}_{\oplus}^{C_i} = \left\{\oplus_{j=1,n}\{F^{A_j^i A_j^i}(\theta_k)\}\right\}_{\theta_k \in [-\pi,\pi[} \quad (14)$$

with $\oplus$ an aggregating operator like min, max, or the mean $\bar{\mu}$. Let $\mathcal{F}^O$ be the Fourier series of the $\mathcal{F}$-signature of an object O to index. If $\exists i / \mathcal{F}_{\min}^{C_i} \subseteq \mathcal{F}^O \subseteq \mathcal{F}_{\max}^{C_i}$, then O is indexed to cluster i, else O is indexed (by default) to cluster $C_{i=\arg\min D\left(\mathcal{F}^O, \mathcal{F}_{\bar{\mu}}^{C_i}\right)}$, with D being the euclidian distance.

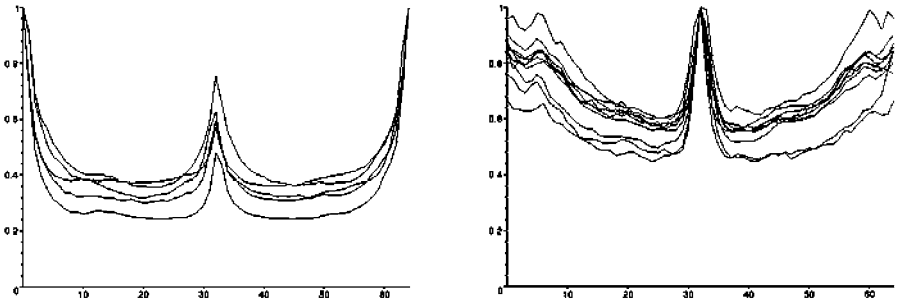

Fig. 4. Some $\mathcal{F}$-signatures of clusters

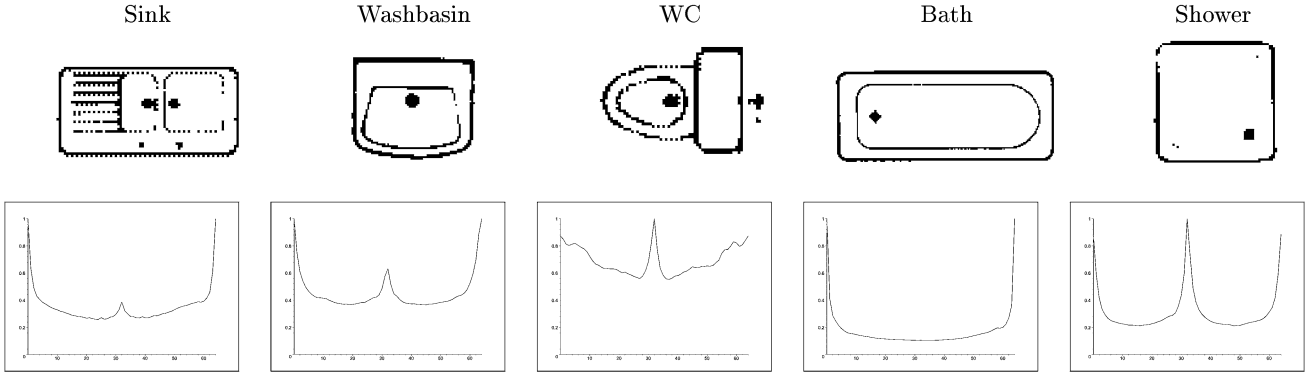

Fig. 5. Samples used and associated $\mathcal{F}$-signatures ($\theta \in [0, \pi[$)

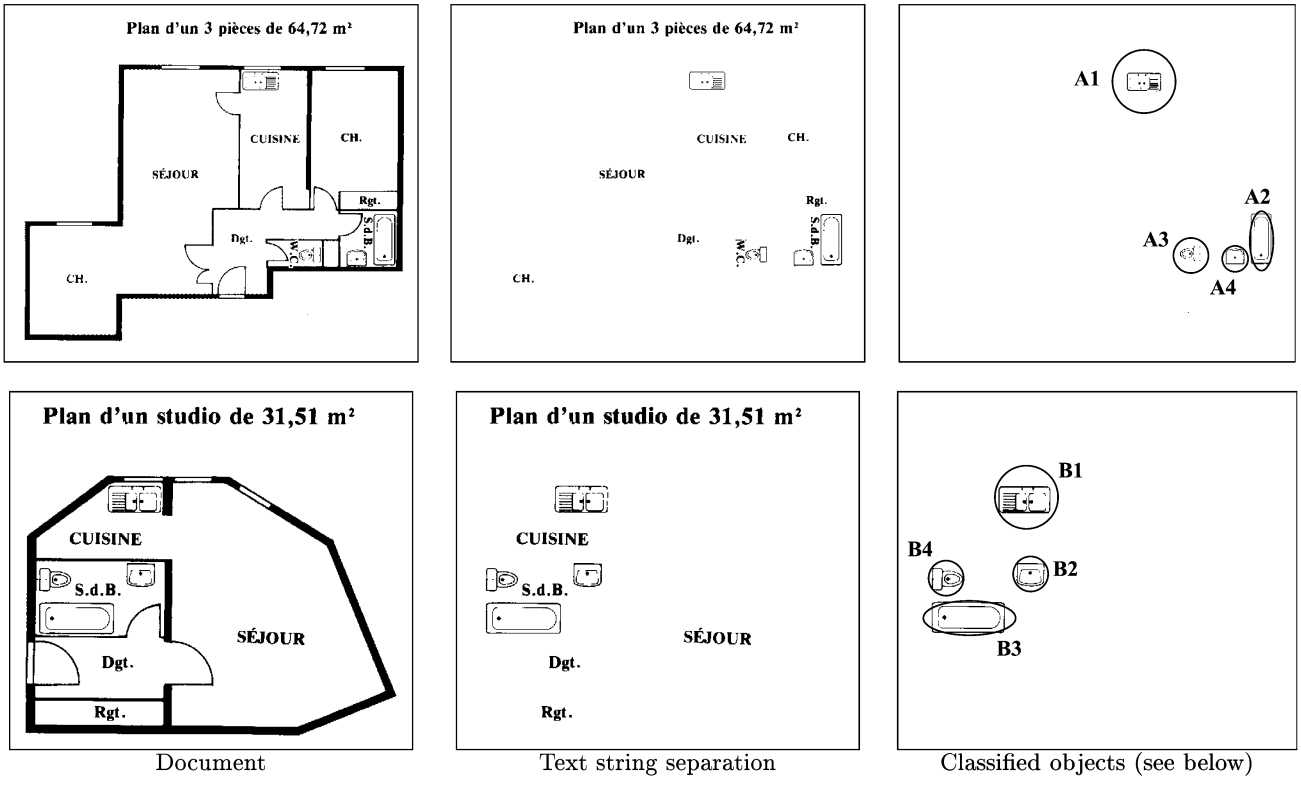

Fig. 6. Recognition of samples

Table 4. Results of the matching process on drawings A and B

Object	A1	A2	A3	A4	B1	B2	B3	B4
Sink	**0.076**	0.257	0.428	0.393	**0.132**	0.241	0.290	0.409
Washbasin	0.226	0.433	0.391	**0.171**	0.233	**0.003**	0.461	0.465
WC	0.500	0.678	**0.058**	0.451	0.464	0.423	0.698	**0.070**
Bath	0.252	**0.080**	0.642	0.637	0.334	0.476	**0.064**	0.675
Shower	0.347	0.526	0.748	0.304	0.478	0.386	0.555	0.770

a) Distance between samples and main graphic objects with our approach

Object	A1	A2	A3	A4	B1	B2	B3	B4
Sink	$8.9E^2$	**2.41**	$3.3E^1$	$4.2E^1$	**0.79**	$6.15E^1$	$1.2E^1$	$4.4E^1$
Washbasin	$7.5E^1$	$4.2E^2$	$4.3E^1$	**0.88**	$9.9E^1$	**0.48**	$2.4E^2$	$5.3E^1$
WC	$5.0E^1$	$4.8E^2$	**1.65**	$2.8E^1$	$6.5E^1$	$4.1E^1$	$1.3E^2$	**2.20**
Bath	**2.5E^1**	$2.5E^3$	$1.1E^2$	$1.6E^2$	$3.0E^1$	$2.3E^2$	**0.67**	$1.5E^2$
Shower	$1.5E^2$	$2.4E^2$	$6.8E^1$	$1.4E^1$	$1.9E^2$	$1.6E^1$	$4.1E^2$	$8.6E^1$

b) Distance between samples and main graphic objects using the Fourier descriptors [22]

Table 5. Results of the matching process on drawing C

Object	C1	C2	C3	C4	C5	C6
Sink	**0.049**	**0.102**	0.378	0.311	0.292	0.269
Washbasin	0.266	0.214	0.265	**0.153**	0.332	0.474
WC	0.539	0.571	**0.179**	0.541	0.715	0.705
Bath	0.216	0.270	0.551	0.559	0.486	**0.076**
Shower	0.361	0.312	0.631	0.249	**0.089**	0.568
reality	Sink	Washb.	WC	Washb.	Shower	Bath

a) Distance between samples and main graphic objects with our approach

Object	C1	C2	C3	C4	C5	C6
Sink	$5.7E^2$	**1.2E^2**	$2.3E^2$	$5.3E^1$	$1.3E^2$	$2.8E^1$
Washbasin	$2.5E^2$	$2.4E^2$	$8.5E^1$	**4.69**	$1.7E^1$	$2.6E^2$
WC	$3.0E^2$	$1.3E^2$	$1.3E^2$	$2.6E^1$	$6.4E^1$	$1.1E^2$
Bath	$1.6E^3$	$2.1E^2$	$6.7E^2$	$2.0E^2$	$4.1E^2$	**1.9E^1**
Shower	**1.3E^2**	$2.9E^2$	**5.0E^1**	$1.3E^1$	**0.22**	$3.3E^2$

b) Distance between samples and main graphic objects using Fourier descriptors [22]

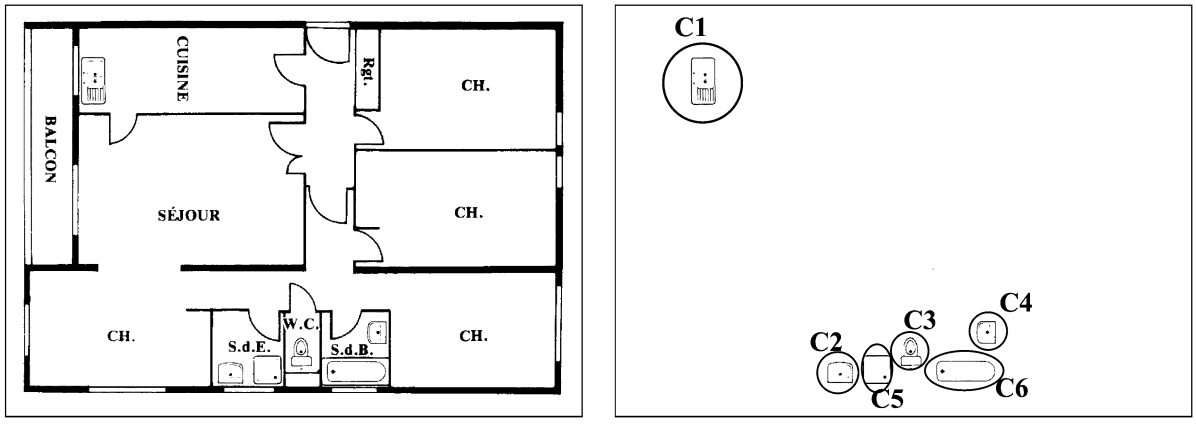

Fig. 7. Example with degraded objects

Fig. 8. Examples of degraded symbols found in documents that require manual closing operation to compute the Fourier descriptors

Table 6. Improvement of the classification using sets of samples for each cluster

Object	Indexing	Proximity	Target cluster
C1	0.130	0.043	Sink
C2	0.112	0.035	Washbasin
C3	0.105	0.062	WC
C4	0.073	0.039	Washbasin
C5	0.015	0.005	Shower
C6	0.102	0.045	Bath

5 Experimental results and discussion

To test the validity of our approach, we have selected five classical objects from an architectural drawing. Figure 5 shows the objects and their associated $\mathcal{F}$-signatures.

The scanned drawings were segmented using an improved version of Fletcher and Kasturi's well-known text-graphics separation method [7,27]. In most cases, text and thin graphics objects representing, respectively, the walls and other objects are correctly segmented with this method. When the text recovery method described in [27] does not disconnect text touching the graphics, a user interface allows the operator to correct the segmentation errors [6]. After this user correction, when several connected components are included in one another, the area on which the $\mathcal{F}$-signature is computed is the largest bounding box.

Each $\mathcal{F}$-signature consists of $p = 128$ values, and K is defined for an error of accuracy set to 10^{-1} for the Fourier series (higher precisions do not lead to significant differences in the final results). Figure 6 presents two examples of architectural documents. Tables 4a and 5a give the results of the indexing process of our approach. The recognized cluster is represented in bold in the result tables. The lowest values indicate the best recognition rates. Scores corresponding to misclassified objects are underlined in the tables. Furthermore, for each document, the area corresponding to an object recognized by the matching is labeled by the recognized cluster on the corresponding figure.

We have compared our approach with that of Rui [22], which is based on Fourier descriptors. The author proposes an adapted version of Fourier descriptors [21] in order to match two objects. Tables 4b and 5b show that the Fourier-based method is less robust than ours, especially for degraded objects (see Fig. 8). One object out of 14 is misclassified (C2) by our approach, whereas 5 out of 14 ($A1$, $A2$, $C1$, $C2$ et $C3$) are misclassified by Rui's approach. This can be explained by the fact that Fourier descriptors are better suited to the description of simple convex shapes, with closed contours. For the sake of comparison, the contours of the objects tested with Fourier descriptors were manually closed, and only the external contour was taken into account.

We have also tested discrete matching using the similarity ratio, as presented in Sect. 4.2. Experimental studies have shown that matching continuous signatures is more robust than the matching of discrete signatures. This robustness was further confirmed on degraded examples. It is obvious that the continuous signature is less subject to noise.

In Table 6, the *Indexing* column gives the nearest signature belonging to the target cluster and the *Proximity* column corresponds to the nearest signature belonging to the cluster. Using such a strategy, all the objects of Fig. 7 are correctly classified (**C2** has been correctly classified in this case).

In a few cases, thin objects connected to a wall are badly segmented. If not recovered through the user interface, the main part of such an object is usually lost. Our approach can overcome this problem in some cases. For example, **C6** (see Fig. 7) is correctly classified, although the external border of the "bath" symbol is missing. Of course, improvements in the segmentation itself would also improve the indexing process. Nevertheless all the objects, except one (F3) of the seven drawings (28 objects) given in the appendix, were correctly classified with our approach.

6 Conclusion

In this paper, we have shown that the force signature can be of great interest for locating and recognizing general graphical symbols in technical line drawings. For each document, areas corresponding to the recognized objects are labeled by the target cluster. The computation of such a feature is fast (low complexity) and gives accurate classifications. The definition of such a layer can allow us to design a system able to use queries such as "search technical documents having more than two WC and one bath." Moreover, more complex queries, including a spatial description of the location of the object based on force histograms, can also be considered [18].

With only the $\mathcal{F}$-signature of one sample per cluster we are able to obtain a fully correct classification when the document is relatively well scanned and binarized. Using degraded objects, results can be ambiguous but are improved by using the whole sample set.

These results are very promising; however, they still need further validation by processing much larger databa-

ses of technical drawings, with more graphical symbols, to assess the discriminating power and the robustness of the method. In this case, it may be necessary to add some indexing scheme, both for efficiency and for discrimination. We are planning to test the construction of a binary search tree associating each node with an $\mathcal{F}$-signature. The use of layer decomposition can also improve the indexing strategy, of course. Finally, we are currently working on extending these results to more powerful and discriminant signatures using the Radon transform [24].

Acknowledgements. The authors are thankful for the many constructive and detailed comments and suggestions provided by the four reviewers of this paper, which helped improve its organization and content.

Appendix – some further results

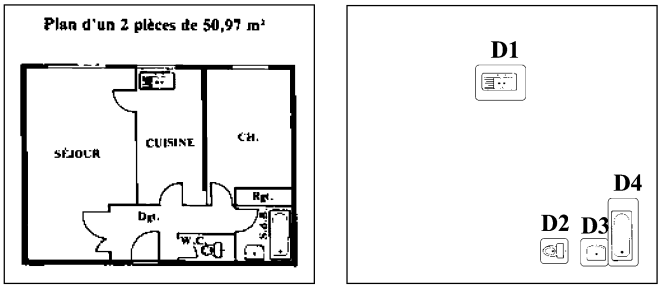

Fig. 9. Example D

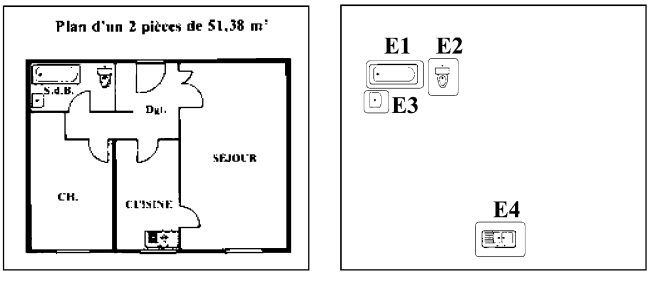

Fig. 10. Example E

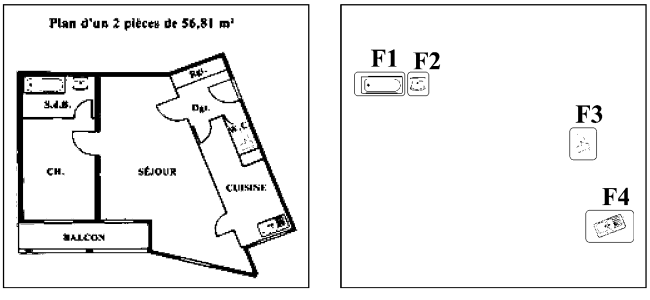

Fig. 11. Example F

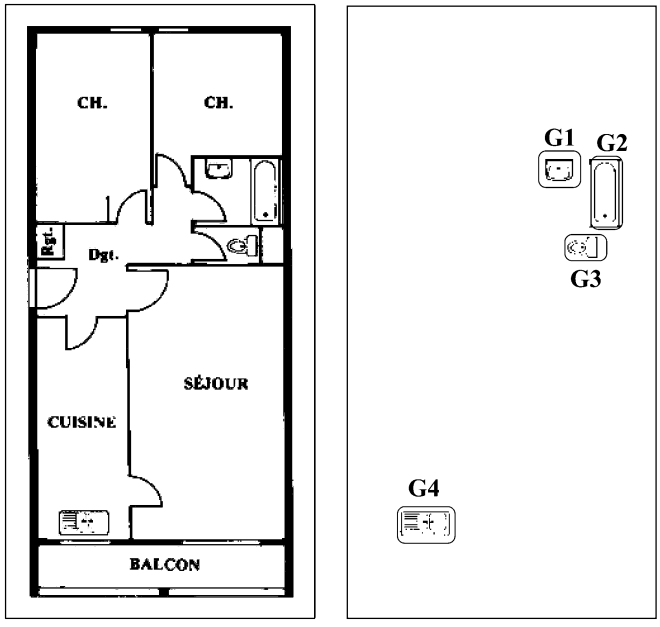

Fig. 12. Example G

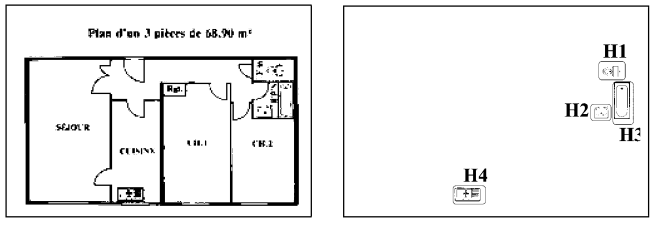

Fig. 13. Example H

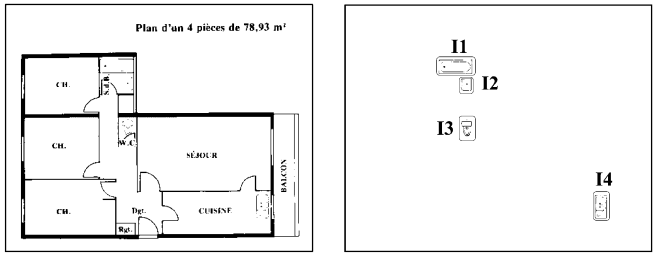

Fig. 14. Example I

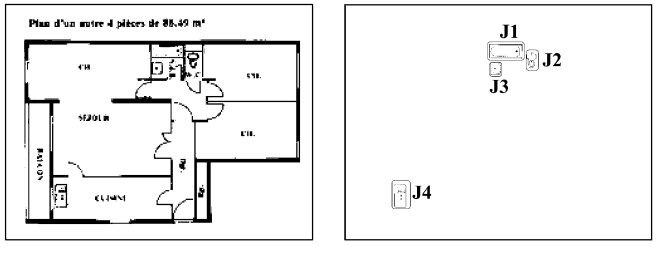

Fig. 15. Example J

Table 7. Results obtained from example D

Object	D1	D2	D3	D4
Score	0.091	0.055	0.156	0.030
Target	Sink	WC	Washb.	Bath

Table 8. Results obtained from example E

Object	E1	E2	E3	E4
Score	0.057	0.060	0.083	0.036
Target	Bath	WC	Washb.	Sink

Table 9. Results obtained from example F

Object	F1	F2	F3	F4
Score	0.034	0.194	0.265	0.171
Target	Bath	WashB.	Washb.	Sink

Table 10. Results obtained from example G

Object	G1	G2	G3	G4
Score	0.173	0.018	0.064	0.052
Target	Washb.	Bath	WC	Sink

Table 11. Results obtained from example H

Object	H1	H2	H3	H4
Score	0.173	0.097	0.054	0.080
Target	WC	Washb.	Bath	Sink

Table 12. Results obtained from example I

Object	I1	I2	I3	I4
Score	0.048	0.212	0.139	0.067
Target	Bath	Washb.	WC	Sink

Table 13. Results obtained from example J

Object	J1	J2	J3	J4
Score	0.029	0.050	0.106	0.118
Target	Bath	Washb.	WC	Sink

References

1. Ballard DH (1981) Generalizing the Hough transform to detect arbitary shapes. Pattern Recog 13(2):111–122
2. Baum LS, Boose JH, Kelley RJ (1998) Graphics recognition for a large-scale airplane information system. In: Tombre K, Chhabra AK (eds) Graphics recognition: algorithms and systems. Lecture notes in computer science, vol 1389. Springer, Berlin Heidelberg New York, pp 291–301
3. Belkasim SO, Shridar M, Ahmadi M (1991) Pattern recognition with moment invariants: a comparative study and new results. Pattern Recog 24:1117–1138
4. Bresenham JE (1965) Algorithm for computer control of a digital plotter. IBM Sys J 4(1):25–30
5. Cordella LP, Vento M (2000) Symbol recognition in documents: a collection of techniques? IJDAR 3(2):73–88
6. Dosch P, Tombre K, Ah-Soon C, Masini G (2000) A complete system for analysis of architectural drawings. IJDAR 3(2):102–116
7. Fletcher LA, Kasturi R (1988) A robust algorithm for text string separation from mixed text/graphics images. IEEE Transactions on PAMI, 10(6):910–918
8. Fränti P, Mednonogov A, Kyrki V, Kälviäinen H (2000) Content-based matching of line-drawing images using the Hough transform. IJDAR 3(2):117–124
9. Gerdes R, Otterbach R, Kammuler R (1995) Fast and robust recognition and localization of 2D objects. Machine Vis Applicat 8:365–374
10. Ghorbel F (1994) A complete invariant description for gray level images by harmonic analysis approach. Pattern Recog Lett 15:1043–1051
11. Kassim AA, Tan T, Tan KH (1999) A comparative study of efficient generalised Hough transform techniques. Image Vision Comput 17:737–748
12. Kauppinen H, Seppänen T, Pietikäinen M (1995) An experimental comparison of autoregressive and Fourier-based descriptors in 2D shape classification. IEEE Transactions on PAMI, 17(2):201–207
13. Krishnapuram R, Keller JM, Ma Y (1993) Quantitative analysis of properties and spatial relations of fuzzy image regions. IEEE Transactions on fuzzy systems, 3(1):222–233
14. Lin BC, Shen J (1991) Fast computation of moment invariants. Pattern Recog 24:807–813
15. Loncaric S (1998) A survey of shape analysis techniques. Pattern Recog 31(8):983–1001
16. Maes M (1991) Polygonal shape recognition using string-matching techniques. Pattern Recog 24(5):433–440
17. Matsakis P (1998) Structural spatial relations and image understanding. Ph.D. thesis (in French), Université de Toulouse III
18. Matsakis P, Keller J, Wendling L, Marjamaa J, Sjahputera O (2001) Linguistic description of relative positions in images. IEEE Transactions on systems, man, and cybernetics – part B, 31(4):573–588
19. Matsakis P, Wendling L (1999) A new way to represent the relative position between areal objects. IEEE Transactions on PAMI, 21(7):634–643
20. Miyajima K, Ralescu A (1994) Spatial organization in 2D segmented images: representation and recognition of primitive spatial relations. Fuzzy Sets Sys 2(65):225–236
21. Persoon E, Fu K (1977) Shape discrimination using Fourier descriptors. IEEE Transactions on systems, man, and cybernetics, 7(3):170–179
22. Rui Y, She A, Huang TS (1998) A modified fourier descriptor for shape matching in mars. In: Chang SK (ed) Image databases and multimedia search. Software engineering and knowledge engineering, vol 8. World Scientific, Singapore, pp 165–180
23. Syeda-Mahmood T (1999) Indexing of technical line drawing databases. IEEE Transactions on PAMI, 21(8):737–751

24. Tabbone S, Wendling L (2002) Technical symbols recognition using the two-dimensional Radon transform. In: Proceedings of the 16th international conference on pattern recognition, August 2002, Québec, 2:200–203
25. Tabbone S, Wendling L, Tombre K (2001) Indexing of technical line drawings based on F-signatures. In: Proceedings of 6th international conference on document analysis and recognition, September 2001, Seattle, pp 1220–1224
26. Teag R (1980) Image analysis via the general theory of moments. J Opt Soc Am 70(8):920–921
27. Tombre K, Tabbone S, Pélissier L, Lamiroy B, Dosch P (2002) Text/graphics separation revisited. In: Lopresti D, Hu J, Kashi R (eds) Proceedings of 5th IAPR international workshop on document analysis systems, August 2002, Princeton. Lecture notes in computer science, vol 2423. Springer, Berlin Heidelberg New York, pp 200–211
28. Wendling L, Tabbone S, Matsakis P (2002) Fast and robust recognition of orbit and sinus drawings using histograms of forces. Pattern Recog Lett 23(14):1687–1693
29. Wood J (1996) Invariant pattern recognition: a review. Pattern Recog 29(1):1–17

Salvatore Tabbone received his Ph.D. in computer science from the Institut National Polytechnique de Lorraine (France) in 1994. His research interests include computer vision, pattern recognition, content-based image retrieval, and document analysis and recognition. He is currently an assistant professor at the University of Nancy2 (France) and a member of the QGAR research project on graphics recognition at the LORIA research center.

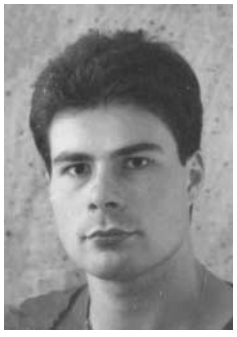

Laurent Wendling received his Ph.D. in computer science from Paul Sabatier University, Toulouse, France in 1997. He worked at the Toulouse Institute of Research in Computer Science, in the Group of Image Processing and Understanding from 1993 to 1999. He is an assistant professor at the Henri-Poincare University, a member of the QGAR team at the LORIA Laboratory in Nancy, and currently in a 2-year senior researcher position at INRIA. His research interests include pattern recognition, graphical document analysis, object retrieval, and graph matching.

Karl Tombre has been professor at Ecole des Mines de Nancy (Institut National Polytechnique de Lorraine) since 1998. From 1987 to 1998, he was senior researcher at INRIA. His main research interest is in the area of analysis and recognition of graphics in technical documents, engineering drawings, maps, etc. Professor Tombre is the leader of the QGAR research project on graphics recognition at the LORIA research center. Since September 2000, he has been secretary of the International Association for Pattern Recognition (IAPR). From 1992 to 1996, he was chairman of IAPR TC10 on graphics recognition. In 1995 and 1997 he cochaired the first two IAPR GREC graphics recognition workshops, was program cochair for ICDAR'99 and ICDAR'01, and is a member of many conference committees. He is one of the editors-in-chief of IJDAR and an advisory editor for the Machine Graphics & Vision journal.